INORGANIC CHEMISTRY FRONTIERS

RESEARCH ARTICLE

View Article Online
View Journal | View Issue

Cite this: *Inorg. Chem. Front.*, 2024, **11**, 4307

Designing promising ultraviolet (UV) birefringent crystals with different hydrogen-bonded phosphate frameworks†

Miao-Bin Xu,[a] Jin Chen, *[a,b] Huai-Yu Wu,[a] Jia-Jia Li,[a] Ning Yu,[a] Mo-Fan Zhuo,[a] Fei-Fei Mao *[b,c] and Ke-Zhao Du [a]

Received 15th May 2024,
Accepted 8th June 2024

DOI: 10.1039/d4qi01220h

rsc.li/frontiers-inorganic

In this study, we computationally identified using first-principles calculations two pyridine derivatives with high polarizability anisotropy: $(C_6H_7N_2O)^+$ (protonated nicotinamide, abbreviated as $3AP^+$) and $(C_6H_6NO_2)^+$ (protonated nicotinic acid, abbreviated as $3CP^+$). Subsequently, we synthesized two novel semiorganic crystals: (3AP) (H_2PO_4) (**I**) and (3CP) (H_2PO_4) (**II**). Both crystals incorporate hydrogen-bonded phosphate frameworks (HPFs), which are constituted by $H_2PO_4^-$ anions linked through O–H···O hydrogen bonds. Compound **I** (*Fdd*2) features one-dimensional (1D) hydrogen-bonded phosphate frameworks (HPFs) that interconnect with 2D $[(3AP)(H_2PO_4)]$ layers, forming a complex 3D network. In contrast, compound **II** (*Pbca*) possesses 2D HPFs that are integrated with $3CP^+$ cations to form a 2D layered network. Compound **I** exhibits a moderate second-harmonic generation (SHG) effect (1 × KH_2PO_4), and a significant birefringence ($\Delta n_{cal.}$: 0.191@1064 nm). Furthermore, compound **II** exhibits both a broad bandgap (4.24 eV) but also an exceptional birefringence ($\Delta n_{exp.}$: 0.284@546 nm), which is the highest value reported among all semiorganic phosphates. This suggests that **II** could be a promising candidate for use as an outstanding ultraviolet (UV) birefringent material.

Introduction

Birefringent crystals are key materials used in the production of optical devices, including polarizers, optical isolators, circulators, and phase retarders.[1–7] Inorganic phosphate crystals, known for their short ultraviolet cutoff edges and good crystal growth habits, represent a classic optoelectronic material.[8–13] KDP (KH_2PO_4) and KTP ($KTiPO_4$) are quintessential examples of phosphates, boasting significant application as nonlinear optical (NLO) materials. However, the high symmetry and weak anisotropy of the PO_4^{3-} tetrahedron often limit inorganic phosphates, resulting in low birefringence and phase mismatch.[14–18] Therefore, the search for phosphates with high birefringence remains an active area of research.

To date, researchers have obtained some metal phosphates with high birefringence (Δn > 0.05) and proposed several effective strategies, including: (1) introducing lone pair electron cations (such as Sn^{2+}, I^{5+}) or d^0 transition metal cations (such as Mo^{6+}, W^{6+}).[19–25] These cations can form the building units with high structural distortion and strong polarizability anisotropy, which is beneficial for enhancing the birefringence of phosphates, such as Sn_2PO_4I ($\Delta n_{cal.}$ = 0.664@546 nm).[21] (2) Partial substitution of O atoms with X groups (including F, S, or $-NH_3$) can break the high symmetry of PO_4^{3-} groups, thereby constructing distorted PO_mX_{4-m} tetrahedra with strong polarizability anisotropy, leading to enhanced birefringence, for example, $NaNH_4PO_3F{\cdot}H_2O$ ($\Delta n_{exp.}$ = 0.053@589.3 nm),[26] KH_2PO_3S ($\Delta n_{cal.}$ = 0.1@1 μm),[27] and $NaPO_3NH_3$ ($\Delta n_{exp.}$ = 0.062@546.1 nm).[28] (3) Combining PO_4^{3-} with traditional planar π-conjugated birefringent functional groups (such as CO_3^{2-} and BO_3^{3-}). This method can increase the birefringence of compounds (Δn > 0.1) while also having a wide bandgap (E_g > 6.2 eV), such as $Sr_3Y(PO_4)(CO_3)_3$ ($\Delta n_{cal.}$ = 0.121@532 nm and E_g = 6.9 eV).[29] Notably, $Rb[PO_2(NH)_3(CO)_2]{\cdot}0.5H_2O$,[30] $KPO_2(NHCONH_2)_2$,[31] and $NaPO_2(NH)_3(CO)_2$ [32] can be regarded as products designed using both methods (2) and (3) concurrently. Of these, $NaPO_2(NH)_3(CO)_2$ exhibits very large birefringence and a wide bandgap ($\Delta n_{exp.}$ = 0.280@550 nm;

[a]*College of Chemistry and Materials Science, Fujian Key Laboratory of Polymer Materials, Fujian Normal University, Fuzhou, 350002 China.*
E-mail: cj2015@fjnu.edu.cn
[b]*State Key Laboratory of Structural Chemistry, Fujian Institute of Research on the Structure of Matter, Chinese Academy of Sciences, Fuzhou, 350002, P. R. China*
[c]*College of Science, Nanjing Agricultural University, Nanjing 210095, P. R. China*

†Electronic supplementary information (ESI) available. CCDC 2343554 and 2343555 for (3AP) (H_2PO_4) (**I**) and (3CP) (H_2PO_4) (**II**). For ESI and crystallographic data in CIF or other electronic format see DOI: https://doi.org/10.1039/d4qi01220h

$E_g \geq 6.5$ eV).[32] (4) The "zipper" arrangement of the PO_4^{3-} tetrahedron with large-angle deviation can also lead to the enhancement of birefringence of metal phosphates. For example, α-$YSc(PO_4)_2$ exhibits deep ultraviolet transmission and a high birefringence ($\Delta n_{cal.}$ = 0.102@1064 nm).[33]

Recently, several semiorganic cations with planar π-conjugated configurations, including $[C(NH_2)_3]^+$, $(C_5H_6ON)^+$, $(C_3H_7N_6)^+$, *etc*., have emerged as high-performance anisotropic functional moieties.[34–37] The combination of π-conjugated organic cations with phosphate tetrahedra has led to the discovery of numerous novel crystals with high birefringence, such as $[C(NH_2)_3]_3PO_4{\cdot}2H_2O$ ($\Delta n_{exp.}$ = 0.055@546 nm),[38] $[C(NH_2)_3]_6(PO_4){\cdot}3H_2O$ ($\Delta n_{exp.}$ = 0.078@546 nm),[39] $(C_3H_7N_6)_6(H_2PO_4)_4(HPO_4){\cdot}4H_2O$ ($\Delta n_{cal.}$ = 0.220@1064 nm),[40] and $(C_5H_6ON)^+(H_2PO_4)^-$ ($\Delta n_{cal.}$ = 0.25@1064 nm).[41] Clearly, as the π-conjugation in organic cations expands, their contribution to birefringence similarly increases significantly. Therefore, we identified two novel birefringent functional units, characterized by higher π-conjugation and stronger polarizability anisotropy, which are $(C_6H_6N_2O)^+$ (protonated 3-carboxamide pyridine, $3AP^+$) and $(C_6H_6NO_2)^+$ (protonated 3-carboxypyridine, $3CP^+$) (Scheme 1). And then, our efforts have resulted in the discovery of two novel semiorganic phosphates, namely $(3AP)(H_2PO_4)$ (**I**) and $(3CP)(H_2PO_4)$ (**II**). Experimental characterization and theoretical calculations have revealed that **I** exhibits large birefringence and moderate SHG effect ($\Delta n_{exp.}$ = 0.196@546 nm; 1.0 × KDP). **II** can serve an excellent UV birefringent crystal with the bandgap of 4.20 eV and birefringence of 0.284@546 nm, the highest value among known semiorganic phosphates.

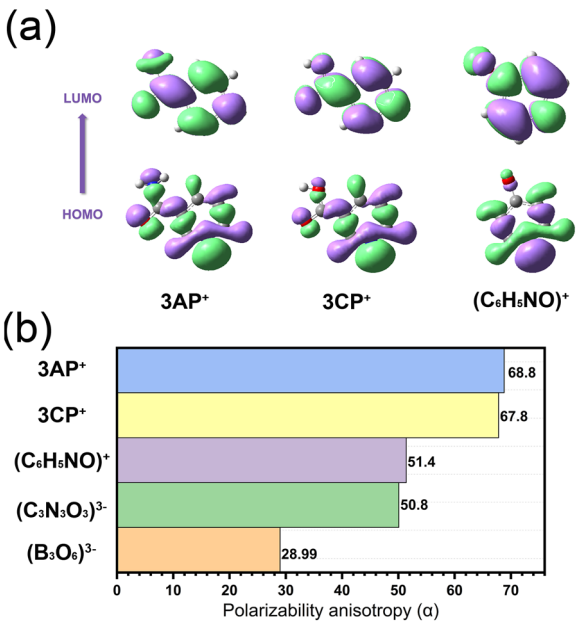

Scheme 1 The HOMO and LUMO maps (a) as well as polarizability anisotropy (b) of related units.

Experimental

Materials and synthesis

$C_6H_6N_2O$ (99%) and H_3PO_4 (85%) were used as purchased from Adamas Beta. Crystals of **I** were synthesized using a simple evaporation technique in aqueous solution. The raw reactants of $C_6H_6N_2O$ (8.2 mmol, 1.00 g) and H_3PO_4 (0.5 mL) were mixed together in deionized water (3 mL) in a glass beaker. The solution was allowed to reach room temperature and then slowly evaporated, resulting in white flaky crystals that precipitated. For the preparation of **II**, the starting materials consisted of $C_6H_6N_2O$ (2 mmol, 244.25 mg), H_3PO_4 (0.5 mL), and H_2O (1 mL). A mixture of the starting materials was placed into Teflon pouches (23 mL) and sealed inside an autoclave, which was heated to 110 °C for 3 days, and then cooled to 30 °C at a rate of 1.6 °C h^{-1}. Colorless flake-like crystals **I** and **II** were obtained with yields of about 80% and 76% (based on $C_6H_6N_2O$), respectively.

Single crystal structure determination

Single-crystal X-ray diffraction data for the title compounds were collected using a Rigaku XtaLAB Synergy-DW dual-wavelength CCD diffractometer, equipped with Cu Kα radiation (λ = 1.54184 Å) at 293 K. Data reduction was performed using CrysAlisPro, and absorption correction, based on the multi-scan method, was applied.[42] The structures of **I** and **II** were determined using direct methods and refined by full-matrix least-squares fitting on F^2 utilizing SHELXL-2014.[43] Anisotropic thermal parameters were applied to refine all non-hydrogen atoms. The structure underwent a check for missing symmetry elements using PLATON, and none were found.[44] Crystallographic data and structural refinements of the compounds are listed in Tables S1–S11.†

Powder X-ray diffraction

Powder X-ray diffraction (PXRD) patterns were recorded on a Rigaku Ultima IV diffractometer with graphite-monochromated Cu Kα radiation over a 2θ range of 10° to 70° with a step size of 0.02°.

Thermal analysis

Thermogravimetric analysis (TGA) and differential thermal analysis (DTA) data were obtained, *via* using a Rigaku TG-DTA 8121 unit under an argon (Ar) atmosphere, at a heating rate of 10 °C min^{-1}, ranging from 30 °C to 800 °C.

Optical measurements

Infrared (IR) spectra were recorded on a Thermo Fisher Scientific Nicolet 5700 FT-IR spectrometer using KBr pellets over a range from 4000 to 400 cm^{-1}.

Ultraviolet–visible (UV-vis) spectra, ranging from 200 to 800 nm, were recorded on a PerkinElmer Lambda 750 UV-vis spectrophotometer. Reflectance spectra were converted to an absorption spectrum using the Kubelka–Munk function.[45]

Second harmonic generation measurements

Powder SHG measurements were taken using a Q-switched Nd:YAG laser generating radiation at 1064 nm according to the method of Kurtz and Perry.[46] Crystalline samples of **I** were sieved into distinct particle-size ranges: 50–70, 70–100, 100–140, 140–200, 200–250, and 250–325 μm. Sieved KDP (KH_2PO_4) samples, within the same particle-size ranges, were used as references.

Birefringence

The optical path difference of the title compounds were characterized using a polarizing microscope (Nikon LV1000) equipped with a Berek compensator.[47] The average wavelength of the light source was 546 nm. Under orthogonal polarization, the two beams of polarized light pass through the crystal at different speeds, producing interference color phenomena after passing through the analyzer. Polarized light with vibration directions parallel to *K*1, *K*2, *K*1′, *K*1″, *K*2′, *K*2″ represents light with different vibration directions. Polarizers are used to filter out light whose vibration directions are not parallel to the analyzer (AA) or polarizer (PP).

The birefringence (Δn) of microcrystals are calculated with the formula: $R = d\cdot(n_s - n_f) = T\cdot\Delta n$. Herein, R is the optical path difference. The n_s represents the refractive index of the slow light, and n_f represents the refractive index of the fast light. Here, T represents the thickness of the tested single crystal.[35]

Elemental analysis

The elemental content was measured on Vario EL Cube elemental analyzer from Elementar Analysensysteme GmbH, Germany. The combustion temperature was 800 °C.

Energy-dispersive X-ray spectroscope

Microprobe elemental analyses and elemental distribution maps were measured using a field-emission scanning electron microscope (Phenom LE) equipped with an energy-dispersive X-ray spectrometer (EDS, Phenom LE).

Computational method

The electronic structures and optical properties of the compounds were computed using the plane-wave pseudopotential method within the framework of density functional theory (DFT), as implemented in the total energy code Cambridge Sequential Total Energy Package (CASTEP).[48,49] For the exchange–correlation functional, we selected the Perdew–Burke–Ernzerhof (PBE) formula within the generalized gradient approximation (GGA).[50] The interactions between the ionic cores and the valence electrons were modeled using norm-conserving pseudopotentials.[51] The following electrons were considered as valence: C-$2s^2 2p^2$, N-$2s^2 2p^3$, O-$2s^2 2p^4$, P-$3s^2 3p^3$, and H-$1s^1$. The basis set was constructed with plane waves up to a cutoff energy of 750 eV. For both compounds, the self-consistent field (SCF) and optical-property calculations utilized a *k*-point separation of 0.04 $Å^{-1}$ for the numerical integration over the Brillouin zone. The *k*-point samplings employed were 4 × 4 × 4 for compound **I** and 2 × 1 × 1 for compound **II**.[48,49]

To investigate the polarizability anisotropy and electronic structure of selected birefringent units, a systematic computational approach was undertaken using the Gaussian 09 software suite.[52] The hybrid B3LYP functional was employed at the 6-31G(d,p) level of theory for these calculations. Subsequent analysis of the computational results was performed using the Multiwfn 3.8 software package.[53] The polarizability anisotropy was quantified based on the static polarizability values.[54]

Results and discussion

Compound **I**, akin to many previously reported semiorganic phosphates, was synthesized by dissolving a specific stoichiometric ratio of nicotinamide ($C_6H_6N_2O$) and phosphoric acid (H_3PO_4) in an aqueous solution, followed by slow evaporation. It should be noted that nicotinamide is easily hydrolyzed to nicotinic acid in aqueous solutions (Fig. S1†), a process that can be accelerated by heating.[55–57] This hydrolysis facilitated the hydrothermal synthesis of compound **II** *via* the reaction involving nicotinamide and H_3PO_4 at 110 °C. The transparent single crystals of **II**, with dimensions of approximately 13 × 7 × 3 mm^3, were observed (Fig. 1). Powder X-ray diffraction (PXRD) analysis confirmed the purity of the synthesized samples (Fig. S2†). Field-emission scanning electron microscopy (FESEM) analyses of both **I** and **II** detected the presence of C, N, O and P elements (Fig. S3†). Elemental analysis provided weight ratios of C : H : N in **I** and **II** as 5.97 : 1.95 : 8.76 and 5.61 : 0.99 : 7.90, respectively, which are congruent with the crystal structure analysis of 6 : 2 : 9 and 6 : 1 : 8, respectively (Table S12†). This agreement corroborates the presence of $(C_6H_7N_2O)^+$ ($3AP^+$) and $(C_6H_6NO_2)^+$ ($3CP^+$) as the organic cations in the structures of **I** and **II**, respectively. The infrared (IR) spectra for **I** and **II** are presented in Fig. S4,† with the detailed assignments of the absorption peaks provided in Table S13,† showing consistency with those of previously reported semiorganic phosphates.[39–41] Thermal analysis demonstrated that the thermal stability of both compounds decompose above 150 °C (Fig. S5†), comparable to other reported crystals, such as $(C_5H_6ON)^+(H_2PO_4)^-$ (166 °C),[41] $(C_3H_7N_6)_6(H_2PO_4)_4(HPO_4)\cdot 4H_2O$ (120 °C),[40] $[C(NH_2)_3]_6(PO_4)\cdot 3H_2O$ and (100 °C).[39]

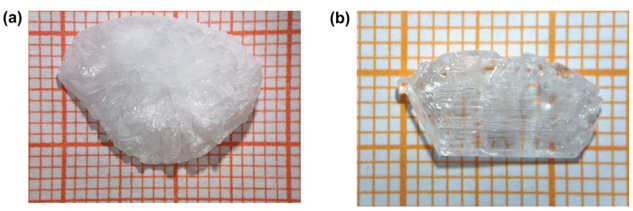

Fig. 1 As-grown crystals of **I** (a) and **II** (b).

Crystal structure

Compound **I** crystallizes in the non-centrosymmetric space group *Fdd*2, with each unit cell housing 16 asymmetric units (Table S1†). Each asymmetric unit consists of one $(C_6H_6N_2O)^+$ ($3AP^+$) cation and one $(H_2PO_4)^-$ anion (Fig. 2a). Within the structure of **I**, each $3AP^+$ cation is interconnected with three $(H_2PO_4)^-$ anions through three N–H···O and one O–H···O hydrogen bonds (Fig. S6a†). Conversely, each $(H_2PO_4)^-$ anion is coordinated with three $3AP^+$ cations *via* three N–H···O hydrogen bonds and is additionally linked to two axial $(H_2PO_4)^-$ anions through two O–H···O hydrogen bonds (Fig. S7a†). Consequently, adjacent $(H_2PO_4)^-$ anions are interconnected *via* O–H···O hydrogen bonds, resulting in the formation of one-dimensional $[H_2PO_4]^-$ chains, denote as 1D hydrogen-bonded phosphate frameworks (1D HPFs) (Fig. 2b). Furthermore, neighboring $3AP^+$ cations and $(H_2PO_4)^-$ anions are connected through hydrogen bonds, creating a 2D neutral layer of $[(3AP)(H_2PO_4)]$ parallel to the *ac* plane (Fig. 2c). Thus, the overall three-dimensional (3D) architecture of **I** can be envisioned as a network of 2D $[(3AP)(H_2PO_4)]$ layers interconnected by 1D HPFs (Fig. 2d).

Compound **II** crystallizes in the centrosymmetric space group *Pbca*, with each unit cell comprising 8 asymmetric units

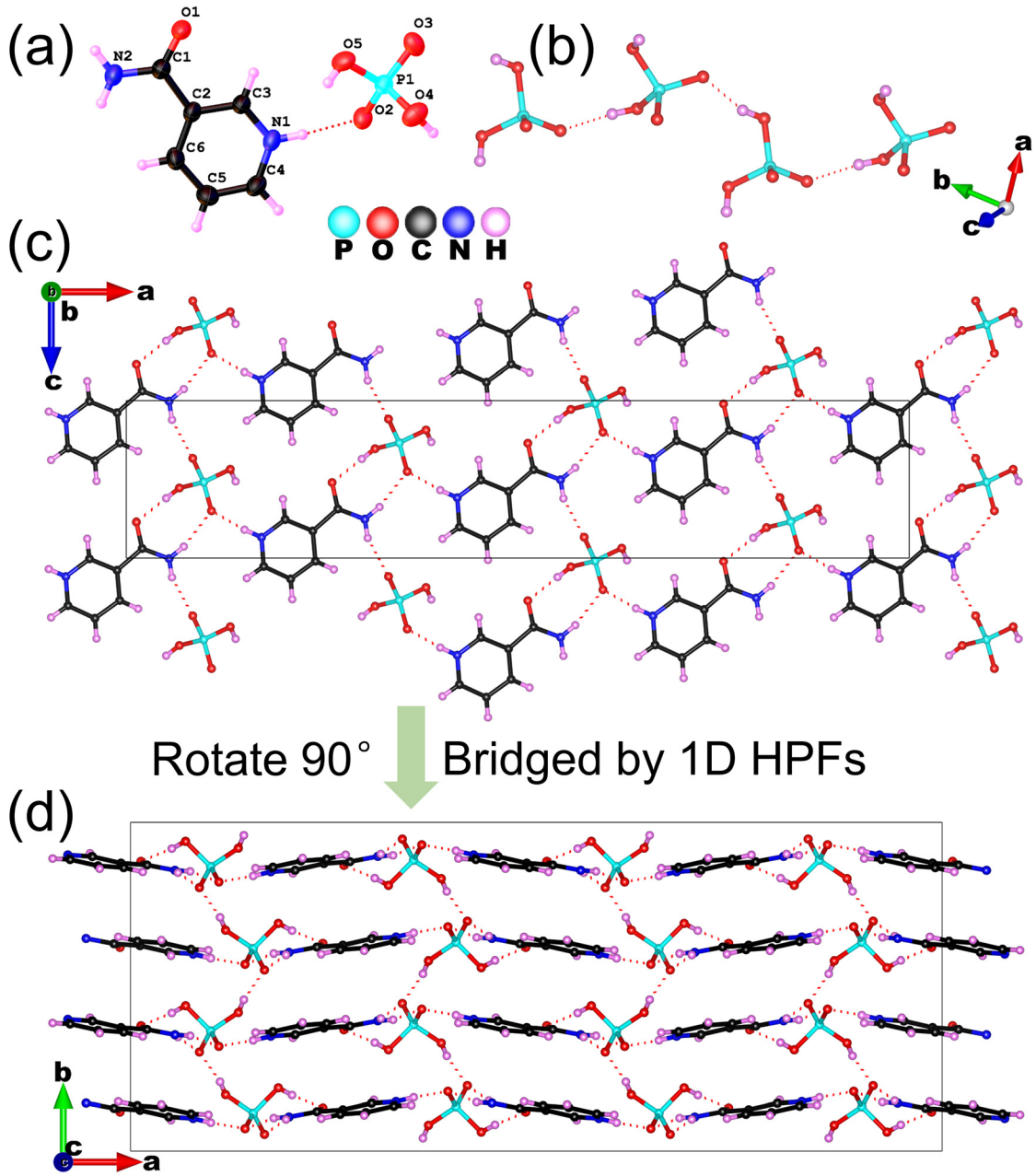

Fig. 2 The asymmetric unit (a), 1D HPFs (b), 2D neutral layer (c) along *b* direction, and 3D overall structure along *c* direction (d).

(Table S1†). Each asymmetric unit consists of one $(C_6H_6NO_2)^+$ ($3CP^+$) cation and one $(H_2PO_4)^-$ anion (Fig. 3a). Within the structure of **II**, pairs of $(H_2PO_4)^-$ anions are interconnected *via* O–H···O hydrogen bonds, forming a $(H_4P_2O_8)^{2-}$ dimer (Fig. S7b†). These dimers further associate through O–H···O hydrogen bonds to create two-dimensional hydrogen-bonded phosphate frameworks (2D HPFs), which are aligned parallel to the *ab* plane (Fig. 3c). Additionally, adjacent $3CP^+$ cations are linked into one-dimensional $[C_6H_6NO_2]^+$ chains through weaker C–H···O hydrogen bonds (Fig. 3b and S6b†). These chains are then integrated with the 2D HPFs through N–H···O and O–H···O hydrogen bonds (Fig. S7b†). Consequently, each pair of cationic 1D $[C_6H_6NO_2]^+$ chains is sequentially embedded on either side of the 2D HPFs, generating a neutral 2D $[(3CP)(H_2PO_4)]$ layer. These 2D layers interlace with each other along the *c*-axis, constituting the overall architecture of compound **II** (Fig. 3d).

We conducted a detailed analysis to discern the differences in π–π and dipole–dipole interactions stemming from the dimensional variation of hydrogen-bonded phosphate frameworks (HPFs). In compound **I**, a π–π interaction along the 1D HPFs is evident, characterized by a plane-to-plane distance of 4.5654(15) Å and a dihedral angle of 15.10(13)° (Fig. S8†). Moreover, adjacent $3AP^+$ cations bordering the 1D HPFs exhibit larger dihedral angles of 24.295°. In contrast, compound **II** displays a π–π interaction along one side of the 2D HPFs with a plane-to-plane distance of 5.0811(13) Å and a dihedral angle of 9.06(11)° (Fig. S9†). Additionally, neighboring $3CP^+$ cations from distinct 2D $[(3CP)(H_2PO_4)]$ layers are nearly antiparallel, with a dihedral angle of 0.12(11)° and a plane-to-

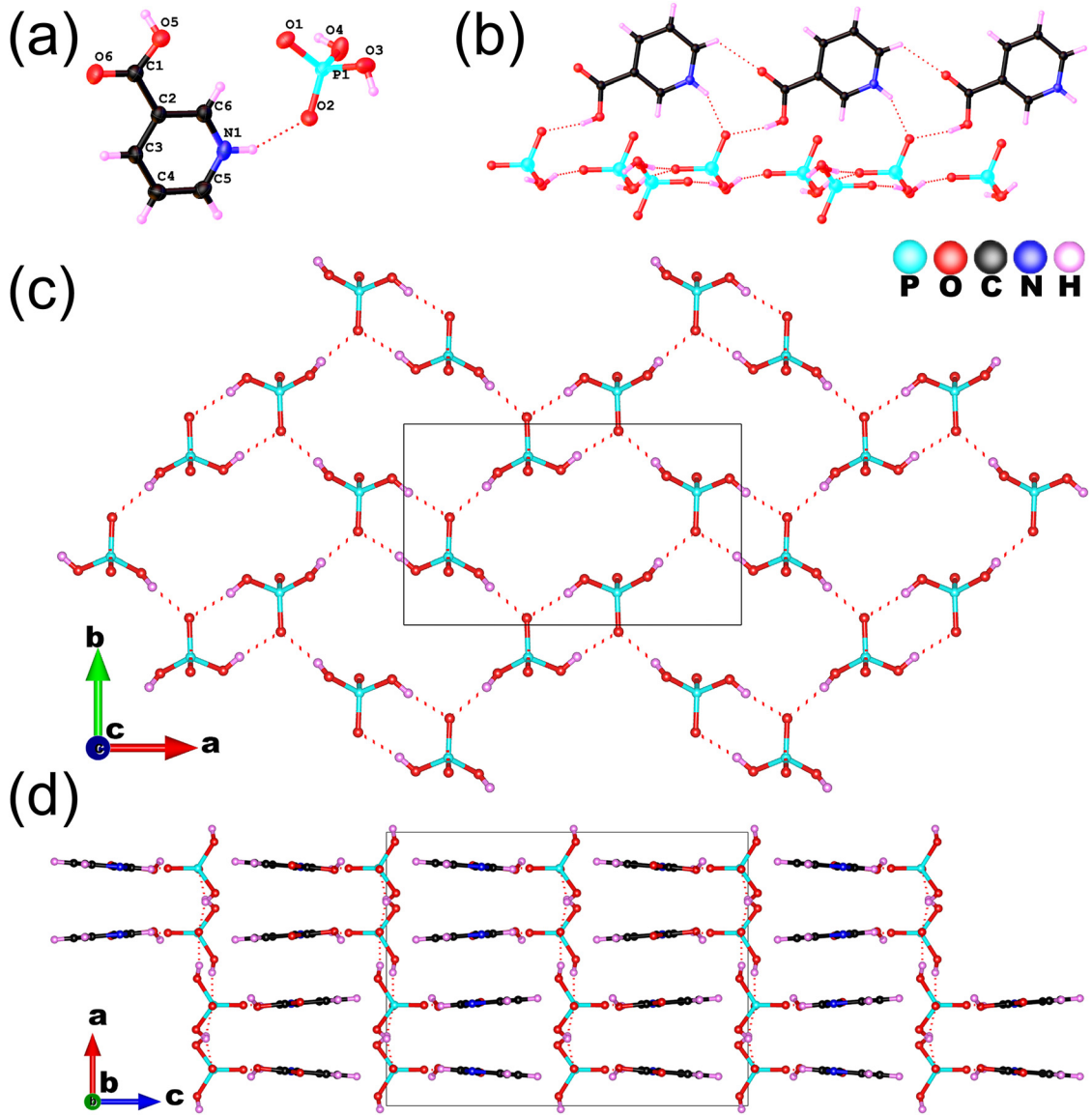

Fig. 3 The asymmetric unit (a), 1D $[C_6H_6NO_2]^+_\infty$ chain (b), 2D HPFs (c) along *c* direction, and overall structure along *b* direction (d).

plane distance of 5.1088(13) Å (Fig. S9†). Notably, this π–π interactions act as the binding force for the stacking of the 2D neutral layers in **II**. Consequently, compound **II** demonstrates stronger dipole–dipole interactions, which may contribute to an enhanced birefringence performance.

Transmittance and bandgaps

Ultraviolet–visible (UV-Vis) absorption spectra indicate that compounds **I** and **II** both exhibit bandgaps of 4.24 eV, with cutoff wavelengths at 265 nm and 270 nm, respectively (Fig. 4a and b). Electronic structure calculations substantiate that the two compounds possess indirect and direct bandgaps, with theoretical values of 2.279 eV and 1.919 eV, respectively (Fig. S10†). To mitigate the systematic underestimation inherent in the Generalized Gradient Approximation (GGA) method when calculating optical properties, scissor operators of 1.921 eV and 2.281 eV are applied. Density of states (DOS) analysis reveals that for both compounds, the top of the valence band predominantly originates from O-2p orbitals, while the conduction band minimum is largely composed of C-2p orbitals, with a minor contribution from N-2p and O-2p orbitals (Fig. 4c and d). This suggests that the bandgaps are mainly shaped by the organic constituents, a finding consistent with previous research on semiorganic phosphates.[39–41]

SHG property

Given that compound **I** crystallizes in a polar space group, we assessed its SHG effect. Upon 1064 nm laser excitation, the SHG intensity of **I** was found to be on par with that of KH_2PO_4 (KDP), utilizing type **I** phase matching (Fig. 5). Compound **I** demonstrates a superior SHG response compared to certain reported semiorganic phosphates, such as $(C_3H_7N_6)_6(H_2PO_4)_4(HPO_4)\cdot 4H_2O$ (0.1 × KDP)[40] and $(C_5H_{12}NO)H_2PO_4$ (0.15 × KDP),[58] and is comparable to $[C(NH_2)_3]_2HPO_4\cdot H_2O$ (1.2 × KDP)[59] and $[C(NH_2)_3]_2PO_3F$ (1.0 × KDP).[60] However, it underperforms in SHG effect relative to [C

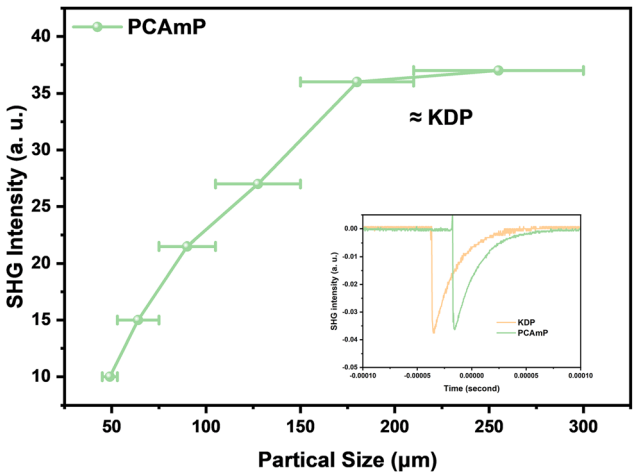

Fig. 5 Phase-matching curve of I with 1064 nm laser radiation (insert is oscilloscope traces of the SHG signals for powders of I and KDP (150–210 μm) with 1064 nm laser radiation).

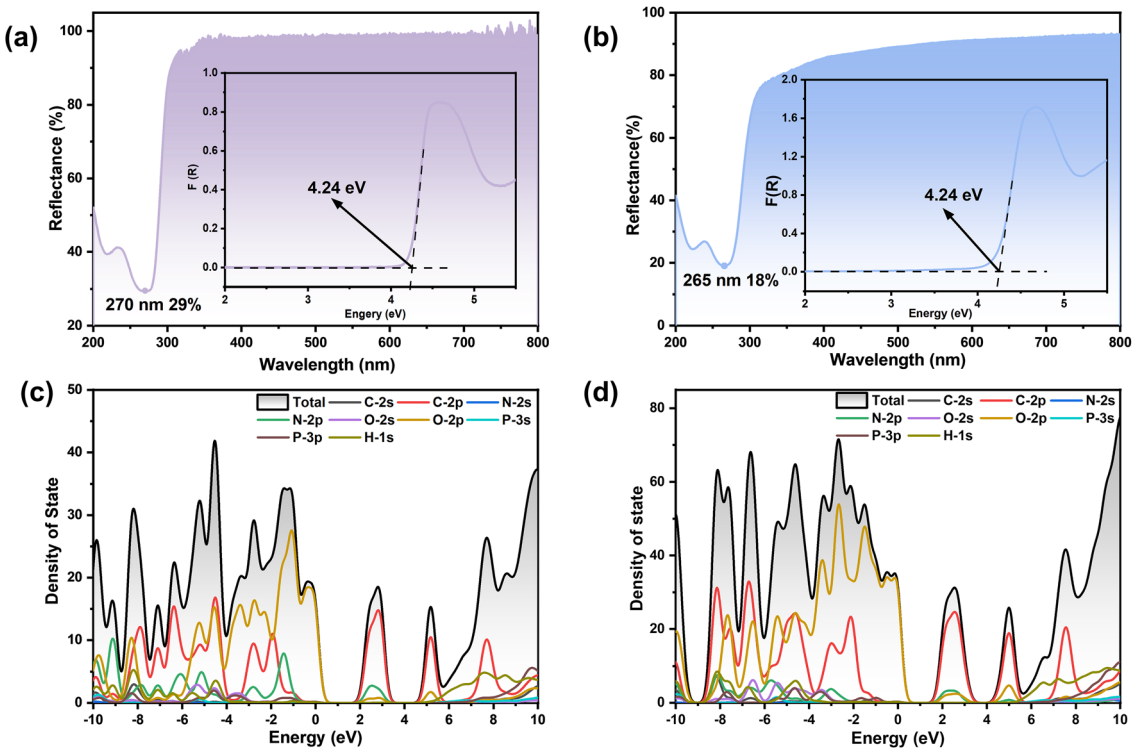

Fig. 4 UV–vis diffuse reflectance spectra (the inset show the bandgaps and *F*(*R*) is absorption coefficient/scattering coefficient.) for I (a) and II (b), as well as the density of states for I (c) and II (d).

$(NH_2)_3]PO_4{\cdot}2H_2O$ (1.5 × KDP),[38] $[C(NH_2)_3]_6(PO_4){\cdot}3H_2O$ (3.8 × KDP),[39] and $(C_5H_6ON)^+(H_2PO_4)^-$ (3.0 × KDP).[41] Additionally, theoretical NLO coefficients for compound **I** were calculated, identifying five non-zero independent tensor components: d_{31} = 0.262 pm V^{-1}, d_{15} = 0.262 pm V^{-1}, d_{32} = 0.087 pm V^{-1}, d_{24} = 0.087 pm V^{-1}, and d_{33} = −0.426 pm V^{-1}. Since the space group of **II** is *Fdd*2, in the *mm*2 point group, its effective tensor should be d_{31}, which is comparable with the measured result.[61–63]

Birefringence property

Using a polarization microscope equipped with a Berek compensator, we measured the optical path difference (R). This measurement is required to determine the transition of the crystals from orthogonal polarization to complete extinction. By applying the formula $R = \Delta n \times T$, where Δn represents the birefringence and T the sample thickness, we obtained the experimental birefringence values for compounds **I** and **II** (Fig. 6). Using a 546 nm laser source, we observed optical path difference of 1007.41 nm for **I** and 1139.46 nm for **II**, corresponding to sample thicknesses of 5.13 μm and 4.01 μm, respectively (Fig. S11†). The resulting birefringence ($\Delta n_{exp.}$) were measured as 0.196 at 546 nm for **I** and 0.284 at 546 nm for **II**. The enhanced birefringence of **II** is attributed to the intensified π–π and dipole–dipole interactions stemming from the smaller dihedral angles between neighboring $3CP^+$ cations within its structure. Notably, the birefringence exhibited by **I** and **II** significantly exceeds the experimental values of recently reported semiorganic phosphates, such as $[C(NH_2)_3]_3PO_4{\cdot}2H_2O$ (0.055@546 nm),[38] $[C(NH_2)_3]_6(PO_4){\cdot}3H_2O$ (0.078@546 nm),[39] $[C(NH_2)_3]_2Sb_3F_3(HPO_3)_4$ (0.027@546 nm),[64] $[C(NH_2)_3]SbFPO_4{\cdot}H_2O$ (0.151@546 nm),[64] $NaIn(C_2O_4)(HPO_4)(H_2O)_5$ (0.098@546 nm),[65] $[Te(C_6H_5)_2][PO_3(OH)]_n$ (0.133@550 nm)[66]

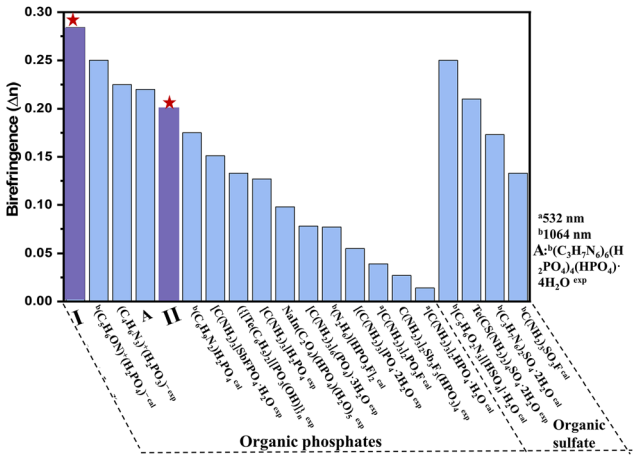

Fig. 7 Birefringence comparison between title compounds and reported phosphates or sulfates containing organic groups.

(Fig. 7 and Table S14†). The increased birefringence of **I** and **II** is primarily due to the enhanced π-conjugation of the $3AP^+$ or $3CP^+$ cations, which introduces greater anisotropy compared to guanidinium or oxalate. Moreover, the experimental birefringence of **II** surpasses that of commercial birefringent crystals, including α-BaB_2O_4 (0.122@532 nm), $CaCO_3$ (0.172@532 nm), and YVO_4 (0.204@532 nm), highlighting its potential as a novel high-performance UV birefringent material.

Subsequently, we computationally determined the dielectric function and refractive indices for compounds **I** and **II**, from which we calculated the theoretical birefringence ($\Delta n_{cal.}$) using the relationships $\varepsilon(\omega) = \varepsilon_1(\omega) + i\varepsilon_2(\omega)$ and $n^2(\omega) = \varepsilon(\omega)$. Both **I** (*Fdd*2) and **II** (*Pbca*) are characterized as biaxial crystals, with their refractive indices ordered as $n_X > n_Y > n_Z$. Specifically, for

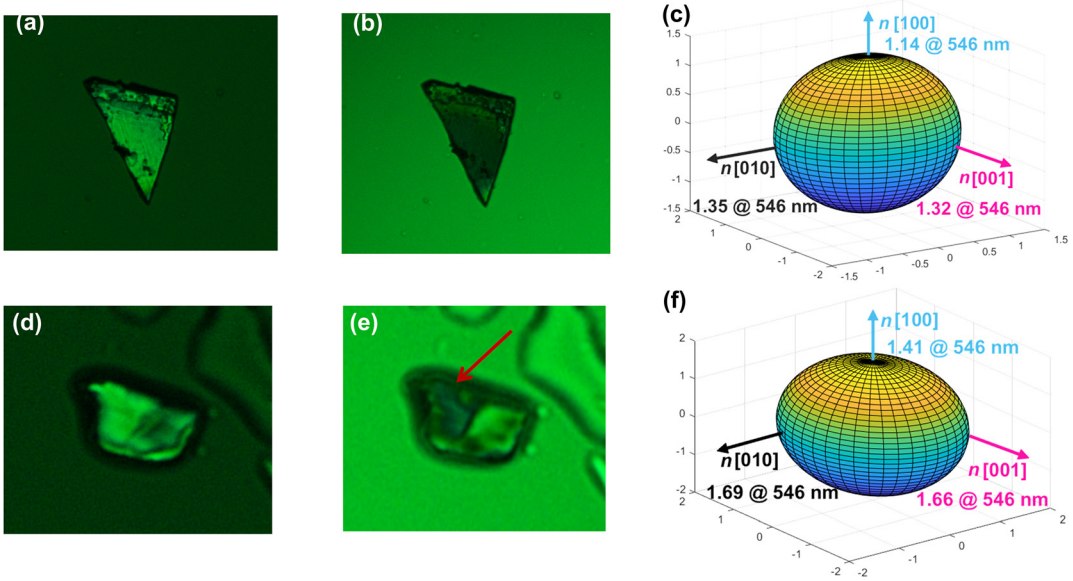

Fig. 6 Original crystal, crystals achieving complete extinction and triaxial ellipsoid of three refractive indices along crystallographic axes for **I** (a–c) and **II** (d–f).

I and **II**, the refractive indices are arranged such that $n[010] > n[001] > n[100]$. To align with the standard crystallographic axes, we performed the transformations [010] → *X*, [001] → *Y*, and [100] → *Z* (Fig. 6 and S12†). At a wavelength of 546 nm, the static refractive indices are as follows: for **I**, $n[100] = 1.14$, $n[010] = 1.35$, $n[001] = 1.32$; and for **II**, $n[100] = 1.41$, $n[010] = 1.69$, $n[001] = 1.66$. The calculated birefringence ($\Delta n_{cal.}$), derived using the formula $\Delta n_{cal.} = n_{max} - n_{min}$, is 0.209 at 546 nm for **I** and 0.284 at 546 nm for **II**, which are consistent with their experimental counterparts. Additionally, the calculated birefringence values at 1064 nm are 0.191 for **I** and 0.264 for **II** (Fig. S12†). Importantly, the calculated birefringence of **II** ($\Delta n_{cal.}$ = 0.286@532 nm and 0.264 nm@1064 nm) exceeds that of currently reported semiorganic phosphates, such as $(C_5H_6ON)^+(H_2PO_4)^-$ (0.25@1064 nm),[41] $[C(NH_2)_3]_2PO_3F$ (0.039@532 nm),[60] $(C_3H_7N_6)_6(H_2PO_4)_4(HPO_4)\cdot 4H_2O$ (0.220@1064 nm),[40] and $(N_2H_6)[HPO_3F]_2$ (0.077@1064 nm)[67] as well as most semiorganic sulfates, including $[C_5H_6O_2N_3][HSO_4]\cdot H_2O$ (0.25@1064 nm),[68] $C(NH_2)_3SO_3F$ (0.133@1064 nm)[69] and $Te(CS(NH_2)_2)_4SO_4\cdot 2H_2O$ (0.210@546.1 nm)[70] (Fig. 7 and Table S14†).

To elucidate the mechanism behind the exceptional birefringence observed in compound **II**, we undertook a computational analysis of the Highest Occupied Molecular Orbital (HOMO) and Lowest Unoccupied Molecular Orbital (LUMO) distributions, complemented by electron localization function (ELF) mapping, as shown in Fig. S13† and Fig. 8. The HOMO is predominantly constituted by O-2p orbitals from the $(H_2PO_4)^-$ group, while the LUMO is significantly influenced by the vacant π-conjugated orbitals of the $3CP^+$ cation, a finding that aligns with the DOS plots. The 2D ELF maps, depicted in Fig. 8a and b, are oriented parallel and perpendicular to the planar $3CP^+$ cation, respectively. These maps reveal significant variations in electron cloud density around the $3CP^+$ cation across different crystallographic planes, in contrast to the relatively uniform electron cloud density observed around the $(H_2PO_4)^-$ anion. By synthesizing the information derived from the LUMO and ELF analyses, we infer that the in-plane and inter-plane anisotropy is predominantly due to the π-conjugated bonds within the $3CP^+$ organic ligands, which are aligned parallel to the (100) crystal plane. This alignment leads to a substantial difference in refractive indices, with $n_{in\text{-}plane} \gg n_{out\text{-}plane}$, consistent with the observed refractive index profile ($n[010] \approx n[001] \gg n[100]$). Therefore, the $3CP^+$ organic ligands are identified as the key contributors to the outstanding birefringence properties of compound **II**.

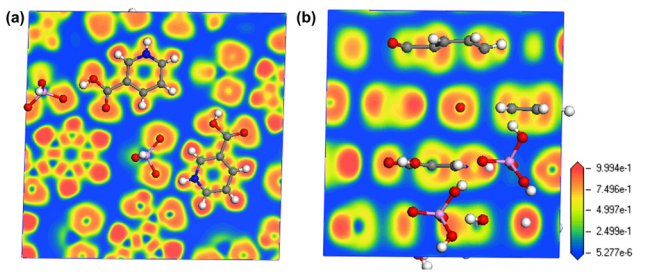

Fig. 8 2D ELF sections projected on crystal planes parallel (a) to and perpendicular (b) to $3CP^+$ cation.

Conclusions

In summary, through the strategic modification of organic cations, we have successfully synthesized two novel semiorganic crystals: $(C_6H_7N_2O)^+(H_2PO_4)^-$ (**I**) with 1D hydrogen-bonded phosphate frameworks (HPFs) and $(C_6H_6NO_2)^+(H_2PO_4)^-$ (**II**) with 2D HPFs. Both compounds exhibit an expansive bandgap of 4.24 eV and remarkable birefringence ($\Delta n_{exp.}$ = 0.196 and 0.284@546 nm for **I** and **II**, respectively). These characteristics position them as prospective candidates for applications in UV birefringent crystals. Structural and computational analyses indicate that the 2D HPFs present in compound **II** augment dipole–dipole interactions and minimize the dihedral angles among the $(C_6H_6NO_2)^+$ cations, subsequently enhancing the birefringence. Given the structural diversity achievable with inorganic frameworks and the compositional flexibility inherent in organic ligands within hybrid organic–inorganic compounds, this study paves the way for further exploration and development of novel high-performance birefringent crystals.

Conflicts of interest

The authors declare no competing financial interest.

Acknowledgements

This work was supported by the National Natural Science Foundation of China (No. 22205037 and 22031009) and Natural Science Foundation of Fujian Province (2023J01498).

References

1 X.-H. Meng, W.-L. Yin and M.-J. Xia, Cyanurates consisting of intrinsic planar π-conjugated 6-membered rings: An emerging source of optical functional materials, *Coord. Chem. Rev.*, 2021, **439**, 213916.
2 A. Tudi, S. Han, Z. Yang and S. Pan, Potential optical functional crystals with large birefringence: Recent advances and future prospects, *Coord. Chem. Rev.*, 2022, **459**, 214380.
3 T. Wu, X. Jiang, K. Duanmu, C. Wu, Z. Lin, Z. Huang, M. G. Humphrey and C. Zhang, Giant Optical Anisotropy in a Covalent Molybdenum Tellurite via Oxyanion Polymerization, *Adv. Sci.*, 2024, **11**, 2306670.
4 P.-F. Li, C.-L. Hu, Y.-F. Li, J.-G. Mao and F. Kong, $Hg_4(Te_2O_5)(SO_4)$: A Giant Birefringent Sulfate Crystal Triggered by a Highly Selective Cation, *J. Am. Chem. Soc.*, 2024, **146**, 7868–7874.

5 J.-H. Wu, C.-L. Hu, T.-K. Jiang, J.-G. Mao and F. Kong, Highly Birefringent d0 Transition Metal Fluoroantimonite in the Mid Infrared Band: Order–Disorder Regulation by Cationic Size, *J. Am. Chem. Soc.*, 2023, **145**, 24416–24424.
6 W.-F. Chen, J.-Y. Lu, J.-J. Li, Y.-Z. Lan, J.-W. Cheng and G.-Y. Yang, $Sr_2[B_5O_8(OH)]_2{\cdot}[B(OH)_3]{\cdot}H_2O$: A Strontium Borate That Shows Deep-Ultraviolet-Transparent Nonlinear Optical Properties, *Chem. – Eur. J.*, 2024, **30**, e202400739.
7 Y.-N. Zhang, Q.-F. Li, B.-B. Chen, Y.-Z. Lan, J.-W. Cheng and G.-Y. Yang, $Na_3B_6O_{10}(HCOO)$: an ultraviolet nonlinear optical sodium borate-formate, *Inorg. Chem. Front.*, 2022, **9**, 5032–5038.
8 Y. Shang, J. Xu, H. Sha, Z. Wang, C. He, R. Su, X. Yang and X. Long, Nonlinear optical inorganic sulfates: The improvement of the phase matching ability driven by the structural modulation, *Coord. Chem. Rev.*, 2023, **494**, 215345.
9 X. Liu, Y.-C. Yang, M.-Y. Li, L. Chen and L.-M. Wu, Anisotropic structure building unit involving diverse chemical bonds: a new opportunity for high-performance second-order NLO materials, *Chem. Soc. Rev.*, 2023, **52**, 8699–8720.
10 H. Fan, N. Ye and M. Luo, New Functional Groups Design toward High Performance Ultraviolet Nonlinear Optical Materials, *Acc. Chem. Res.*, 2023, **56**, 3099–3109.
11 Y. Li, J. Luo and S. Zhao, Local Polarity-Induced Assembly of Second-Order Nonlinear Optical Materials, *Acc. Chem. Res.*, 2022, **55**, 3460–3469.
12 M. Mutailipu, Z. Yang and S. Pan, Toward the Enhancement of Critical Performance for Deep-Ultraviolet Frequency-Doubling Crystals Utilizing Covalent Tetrahedra, *Acc. Mater. Res.*, 2021, **2**, 282–291.
13 X. Chen, Y. Li, J. Luo and S. Zhao, Recent advances in non-π-conjugated nonlinear optical sulfates with deep-UV absorption edge, *Chin. J. Struct. Chem.*, 2023, **42**, 100044.
14 B. L. Wu, C. L. Hu, F. F. Mao, R. L. Tang and J. G. Mao, Highly Polarizable Hg^{2+} Induced a Strong Second Harmonic Generation Signal and Large Birefringence in $LiHgPO_4$, *J. Am. Chem. Soc.*, 2019, **141**, 10188–10192.
15 S. Zhao, X. Yang, Y. Yang, X. Kuang, F. Lu, P. Shan, Z. Sun, Z. Lin, M. Hong and J. Luo, Non-Centrosymmetric $RbNaMgP_2O_7$ with Unprecedented Thermo-Induced Enhancement of Second Harmonic Generation, *J. Am. Chem. Soc.*, 2018, **140**, 1592–1595.
16 Z. Fang, W.-H. Ma, Q.-Y. Chen, X.-T. Zhu, X.-M. Zeng, P.-B. Li, Q.-F. Zhou, T.-T. Song and M.-H. Duan, From $(NH_4)_3[Zr(PO_4)_2F]$ to $(NH_4)_3[Sn_2(PO_4)_2]Cl$: the rational design of a tin-based short-wave ultraviolet phosphate with large optical anisotropy, *Inorg. Chem. Front.*, 2024, **11**, 1775–1780.
17 T. Zheng, Q. Wang, J.-X. Ren, L.-L. Cao, L. Huang, D.-J. Gao, J. Bi and G.-H. Zou, Halogen regulation triggers structural transformation from centrosymmetric to noncentrosymmetric switches in tin phosphate halides Sn_2PO_4X (X = F, Cl), *Inorg. Chem. Front.*, 2022, **9**, 4705–4713.
18 H.-Y. Wu, C.-L. Hu, M.-B. Xu, Q.-Q. Chen, N. Ma, X.-Y. Huang, K.-Z. Du and J. Chen, From $H_{12}C_4N_2CdI_4$ to $H_{11}C_4N_2CdI_3$: a highly polarizable $CdNI_3$ tetrahedron induced a sharp enhancement of second harmonic generation response and birefringence, *Chem. Sci.*, 2023, **14**, 9533–9542.
19 X.-H. Zhang, B.-P. Yang, J. Chen, C.-L. Hu, Z. Fang, Z. Wang and J.-G. Mao, A new iodate-phosphate $Pb_2(IO_3)(PO_4)$ achieving great improvement in birefringence activated by $(IO_3)^-$ groups, *Chem. Commun.*, 2020, **56**, 635–638.
20 M. Ji, C. Hu, Z. Fang, Y. Chen and J. Mao, Tin(II)-Induced Large Birefringence Enhancement in Metal Phosphates, *Inorg. Chem.*, 2021, **60**, 15744–15750.
21 J. Guo, A. Tudi, S. Han, Z. Yang and S. Pan, Sn_2PO_4I: An Excellent Birefringent Material with Giant Optical Anisotropy in Non π-Conjugated Phosphate, *Angew. Chem., Int. Ed.*, 2021, **60**, 24901–24904.
22 X. Lu, Z. Chen, X. Shi, Q. Jing and M. H. Lee, Two Pyrophosphates with Large Birefringences and Second-Harmonic Responses as Ultraviolet Nonlinear Optical Materials, *Angew. Chem., Int. Ed.*, 2020, **59**, 17648–17656.
23 Y. Deng, L. Huang, X. Dong, L. Wang, K. M. Ok, H. Zeng, Z. Lin and G. Zou, $K_2Sb(P_2O_7)F$: Cairo Pentagonal Layer with Bifunctional Genes Reveal Optical Performance, *Angew. Chem., Int. Ed.*, 2020, **59**, 21151–21156.
24 T. Baiheti, S. Han, A. Tudi, Z. Yang and S. Pan, Polar polymorphism: α- and β-$KCsWP_2O_9$ nonlinear optical materials with a strong second harmonic generation response, *J. Mater. Chem. C*, 2020, **8**, 11441–11448.
25 T. Baiheti, S. Han, A. Tudi, Z. Yang and S. Pan, Alignment of Polar Moieties Leading to Strong Second Harmonic Response in $KCsMoP_2O_9$, *Chem. Mater.*, 2020, **32**, 3297–3303.
26 J. Lu, J.-N. Yue, L. Xiong, W.-K. Zhang, L. Chen and L.-M. Wu, Uniform Alignment of Non-π-Conjugated Species Enhances Deep Ultraviolet Optical Nonlinearity, *J. Am. Chem. Soc.*, 2019, **141**, 8093–8097.
27 X. Zhang, L. Kang, P. Gong, Z. Lin and Y. Wu, Nonlinear Optical Oxythiophosphate Approaching the Good Balance with Wide Ultraviolet Transparency, Strong Second Harmonic Effect, and Large Birefringence, *Angew. Chem., Int. Ed.*, 2021, **60**, 6386–6390.
28 L. Wu, H. Tian, C. Lin, X. Zhao, H. Fan, P. Dong, S. Yang, N. Ye and M. Luo, Optimized arrangement of non-π-conjugated PO_3NH_3 units leads to enhanced ultraviolet optical nonlinearity in $NaPO_3NH_3$, *Inorg. Chem. Front.*, 2024, **11**, 1145–1152.
29 L. Xiong, L.-M. Wu and L. Chen, A General Principle for DUV NLO Materials: π-Conjugated Confinement Enlarges Band Gap**, *Angew. Chem., Int. Ed.*, 2021, **60**, 25063–25067.
30 X. Song, Z. Du, B. Ahmed, Y. Li, Y. Zhou, Y. Song, W. Huang, J. Zheng, J. Luo and S. Zhao, A UV solar-blind nonlinear optical crystal with confined π-conjugated groups, *Inorg. Chem. Front.*, 2023, **10**, 5462–5467.
31 F. Chen, F. Mo, H. Chen, M.-J. Lin and Y. Chen, $KPO_2(NHCONH_2)_2$: A Promising Deep-Ultraviolet Nonlinear Optical Phosphate Containing Polar $[PO_2(NHCONH_2)_2]^-$ Tetrahedra, *Chem. Mater.*, 2024, **36**, 2985–2992.

32 Y. Zhou, X. Zhang, M. Hong, J. Luo and S. Zhao, Achieving effective balance between bandgap and birefringence by confining π-conjugation in an optically anisotropic crystal, *Sci. Bull.*, 2022, **67**, 2276–2279.
33 B.-H. Lei, Z. Yang, H. Yu, C. Cao, Z. Li, C. Hu, K. R. Poeppelmeier and S. Pan, Module-Guided Design Scheme for Deep-Ultraviolet Nonlinear Optical Materials, *J. Am. Chem. Soc.*, 2018, **140**, 10726–10733.
34 M. Mutailipu, J. Han, Z. Li, F. Li, J. Li, F. Zhang, X. Long, Z. Yang and S. Pan, Achieving the full-wavelength phase-matching for efficient nonlinear optical frequency conversion in $C(NH_2)_3BF_4$, *Nat. Photonics*, 2023, **17**, 694–701.
35 W.-Q. Huang, X. Zhang, Y.-Q. Li, Y. Zhou, X. Chen, X.-Q. Li, F.-F. Wu, M.-C. Hong, J.-H. Luo and S.-G. Zhao, A Hybrid Halide Perovskite Birefringent Crystal, *Angew. Chem., Int. Ed.*, 2022, **61**, e202202746.
36 Q. Q. Chen, C. L. Hu, J. Chen, Y. L. Li, B. X. Li and J. G. Mao, $[o\text{-}C_5H_4NHOH]_2[I_7O_{18}(OH)]\cdot 3H_2O$: An Organic-Inorganic Hybrid SHG Material Featuring an $[I_7O_{18}(OH)]$ infinity 2 - Branched Polyiodate Chain, *Angew. Chem., Int. Ed.*, 2021, **60**, 17426–17429.
37 Z.-P. Zhang, X. Liu, X. Liu, Z.-W. Lu, X. Sui, B.-Y. Zhen, Z. Lin, L. Chen and L.-M. Wu, Driving Nonlinear Optical Activity with Dipolar 2-Aminopyrimidinium Cations in $(C_4H_6N_3)^+(H_2PO_3)^-$, *Chem. Mater.*, 2022, **34**, 1976–1984.
38 X. Wen, C. Lin, M. Luo, H. Fan, K. Chen and N. Ye, $[C(NH_2)_3]_3PO_4\cdot 2H_2O$: A new metal-free ultraviolet nonlinear optical phosphate with large birefringence and second-harmonic generation response, *Sci. China Mater.*, 2021, **64**, 2008–2016.
39 C. Wu, X. Jiang, Z. Wang, H. Sha, Z. Lin, Z. Huang, X. Long, M. G. Humphrey and C. Zhang, UV Solar-Blind-Region Phase-Matchable Optical Nonlinearity and Anisotropy in a π-Conjugated Cation-Containing Phosphate, *Angew. Chem., Int. Ed.*, 2021, **60**, 14806–14810.
40 S.-F. Li, L. Hu, Y. Ma, F.-F. Mao, J. Zheng, X.-D. Zhang and D. Yan, Noncentrosymmetric $(C_3H_7N_6)_6(H_2PO_4)_4(HPO_4)\cdot 4H_2O$ and Centrosymmetric $(C_3H_7N_6)_2SO_4\cdot 2H_2O$: Exploration of Acentric Structure by Combining Planar and Tetrahedral Motifs via Hydrogen Bonds, *Inorg. Chem.*, 2022, **61**, 10182–10189.
41 J. Lu, X. Liu, M. Zhao, X.-B. Deng, K.-X. Shi, Q.-R. Wu, L. Chen and L.-M. Wu, Discovery of NLO Semiorganic $(C_5H_6ON)^+(H_2PO_4)^-$: Dipole Moment Modulation and Superior Synergy in Solar-Blind UV Region, *J. Am. Chem. Soc.*, 2021, **143**, 3647–3654.
42 R. H. Blessing, An empirical correction for absorption anisotropy, *Acta Crystallogr., Sect. A: Found. Crystallogr.*, 1995, **51**, 33–38.
43 G. M. Sheldrick, Crystal structure refinement with *SHELXL*, *Acta Crystallogr., Sect. C: Struct. Chem.*, 2015, **71**, 3–8.
44 A. Spek, Single-crystal structure validation with the program *PLATON*, *J. Appl. Crystallogr.*, 2003, **36**, 7–13.
45 P. Kubelka and F. Munk, An article on optics of paint layers, *Z. Tech. Phys.*, 1931, **12**, 259–274.
46 S. K. Kurtz and T. T. Perry, A Powder Technique for the Evaluation of Nonlinear Optical Materials, *J. Appl. Phys.*, 1968, **39**, 3798–3813.
47 L. Cao, G. Peng, W. Liao, T. Yan, X. Long and N. Ye, A microcrystal method for the measurement of birefringence, *CrystEngComm*, 2020, **22**, 1956–1961.
48 M. D. Segall, P. J. D. Lindan, M. J. Probert, C. J. Pickard, P. J. Hasnip, S. J. Clark and M. C. Payne, First-principles simulation: ideas, illustrations and the CASTEP code, *J. Phys.: Condens. Matter*, 2002, **14**, 2717.
49 V. Milman, B. Winkler, J. A. White, C. J. Pickard, M. C. Payne, E. V. Akhmatskaya and R. H. Nobes, Electronic structure, properties, and phase stability of inorganic crystals: A pseudopotential plane-wave study, *J. Quantum Chem.*, 2000, **77**, 895–910.
50 J. P. Perdew, K. Burke and M. Ernzerhof, Generalized gradient approximation made simple, *Phys. Rev. Lett.*, 1996, **77**, 3865.
51 J. S. Lin, A. Qteish, M. C. Payne and V. Heine, Optimized and transferable nonlocal separable *ab initio* pseudopotentials, *Phys. Rev. B: Condens. Matter Mater. Phys.*, 1993, **47**, 4174.
52 M. J. Frisch, G. W. Trucks, H. B. Schlegel, G. E. Scuseria, M. A. Robb, J. R. Cheeseman, G. Scalmani, V. Barone, B. Mennucci and G. A. Petersson, *Gaussian 09, Revision B.01*, 2010.
53 T. Lu and F. Chen, Multiwfn: A multifunctional wavefunction analyzer, *J. Comput. Chem.*, 2012, **33**, 580–592.
54 A. Alparone, Linear and nonlinear optical properties of nucleic acid bases, *Chem. Phys.*, 2013, **410**, 90–98.
55 S. Mahesh, K. C. Tang and M. Raj, Amide Bond Activation of Biological Molecules, *Molecules*, 2018, **23**, 2615.
56 G. Li, P. Lei and M. Szostak, Transition-Metal-Free Esterification of Amides via Selective N-C Cleavage under Mild Conditions, *Org. Lett.*, 2018, **20**, 5622–5625.
57 J. I. Mujika, J. M. Mercero and X. Lopez, Water-Promoted Hydrolysis of a Highly Twisted Amide:Rate Acceleration Caused by the Twist of the Amide Bond, *J. Am. Chem. Soc.*, 2005, **127**, 4445–4453.
58 D. Wang, X. Meng, N. Zhang, D. Sun, R. Hou, H. Chen and X. Liu, Characteristics of structure, thermal stability and optical properties for a novel NLO crystal $(C_5H_{12}NO)H_2PO_4$, *Opt. Mater.*, 2023, **135**, 113225.
59 I. Němec, I. Matulková, P. Held, J. Kroupa, P. Němec, D. Li, L. Bohatý and P. Becker, Crystal growth, crystal structure, vibrational spectroscopy, linear and nonlinear optical properties of guanidinium phosphates, *Opt. Mater.*, 2017, **69**, 420–431.
60 L. Xiong, J. Chen, J. Lu, C.-Y. Pan and L.-M. Wu, Monofluorophosphates: A New Source of Deep-Ultraviolet Nonlinear Optical Materials, *Chem. Mater.*, 2018, **30**, 7823–7830.
61 V. G. Dmitriev and D. N. Nikogosyan, Effective nonlinearity coefficients for three-wave interactions in biaxial crystal of mm2 point group symmetry, *Opt. Commun.*, 1993, **95**, 173–182.

62 Z. Chen, Z. Zhang, X. Dong, Y. Shi, Y. Liu and Q. Jing, Li_3VO_4: A Promising Mid-Infrared Nonlinear Optical Material with Large Laser Damage Threshold, *Cryst. Growth Des.*, 2017, **17**, 2792–2800.

63 T. Abudouwufu, M. Zhang, S.-C. Cheng, Z.-H. Yang and S.-L. Pan, $Ce(IO_3)_2F_2{\cdot}H_2O$: The First Rare-Earth-Metal Iodate Fluoride with Large Second Harmonic Generation Response, *Chem. – Eur. J.*, 2018, **25**, 1221–1226.

64 X. Dong, Y. Long, L. Huang, L. Cao, D. Gao, J. Bi and G. Zou, Large optical anisotropy differentiation induced by the anion-directed regulation of structures, *Inorg. Chem. Front.*, 2022, **9**, 6441–6447.

65 X. Zhang, Y. Xue, L. Yang, C. Wu, Z. Huang, J. Xu, M. G. Humphrey and C. Zhang, $NaIn(C_2O_4)(HPO_4)(H_2O)_5$: An Ultraviolet Transparent Nonlinear Optical Oxalate-Phosphate with Large Birefringence, *SSRN*, 2022, **253**, 4056766.

66 M. Xue, L. Zhang, X. Wang, Q. Dong, Z. Zhu, X. Wang, Q. Gu, F. Kang, X.-X. Li and Q. Zhang, A Metal-Free Helical Covalent Inorganic Polymer: Preparation, Crystal Structure and Optical Properties, *Angew. Chem., Int. Ed.*, 2024, **63**, e202315338.

67 H. Qiu, F. Li, C. Jin, J. Lu, Z. Yang, S. Pan and M. Mutailipu, $(N_2H_6)[HPO_3F]_2$: maximizing the optical anisotropy of deep-ultraviolet fluorophosphates, *Chem. Commun.*, 2022, **58**, 5594–5597.

68 L. Zhang, X. Zhang, F. Liang, Z. Hu and Y. Wu, Rational Design of Noncentrosymmetric Organic–Inorganic Hybrids with a π-Conjugated Pyridium-Type Cation for High Nonlinear-Optical Performance, *Inorg. Chem.*, 2023, **62**, 14518–14522.

69 M. Luo, C. Lin, D. Lin and N. Ye, Rational Design of the Metal-Free $KBe_2BO_3F_2$ (KBBF) Family Member $C(NH_2)_3SO_3F$ with Ultraviolet Optical Nonlinearity, *Angew. Chem., Int. Ed.*, 2020, **59**, 15978–15981.

70 X. Weng, C. Lin, G. Peng, H. Fan, X. Zhao, K. Chen, M. Luo and N. Ye, $Te(CS(NH_2)_2)_4SO_4{\cdot}2H_2O$: A Three-in-One Semiorganic Nonlinear Optical Crystal with an Unusual Quadrilateral $(TeS_4)^{6-}$ Chromophore, *Cryst. Growth Des.*, 2021, **21**, 2596–2601.